



Volatile emissions and gas geochemistry of Hot Spring Basin, Yellowstone National Park, USA

C. Werner^{a,*}, S. Hurwitz^b, W.C. Evans^b, J.B. Lowenstern^b, D. Bergfeld^b, H. Heasler^c, C. Jaworowski^c, A. Hunt^d

^a US Geological Survey, Vancouver, WA, United States

^b US Geological Survey, Menlo Park, CA, United States

^c Yellowstone Center for Resources, Yellowstone National Park, Mammoth, WY, United States

^d US Geological Survey, Denver, CO, United States

ARTICLE INFO

Article history:

Received 24 June 2008

Accepted 25 September 2008

Available online 11 October 2008

Keywords:

gas geochemistry

carbon dioxide

hydrogen sulfide

flux

emission

fumarole

Yellowstone

ABSTRACT

We characterize and quantify volatile emissions at Hot Spring Basin (HSB), a large acid-sulfate region that lies just outside the northeastern edge of the 640 ka Yellowstone Caldera. Relative to other thermal areas in Yellowstone, HSB gases are rich in He and H₂, and mildly enriched in CH₄ and H₂S. Gas compositions are consistent with boiling directly off a deep geothermal liquid at depth as it migrates toward the surface. This fluid, and the gases evolved from it, carries geochemical signatures of magmatic volatiles and water–rock reactions with multiple crustal sources, including limestones or quartz-rich sediments with low K/U (or ⁴⁰Ar/⁴He). Variations in gas chemistry across the region reflect reservoir heterogeneity and variable degrees of boiling. Gas-geothermometer temperatures approach 300 °C and suggest that the reservoir feeding HSB is one of the hottest at Yellowstone. Diffuse CO₂ flux in the western basin of HSB, as measured by accumulation-chamber methods, is similar in magnitude to other acid-sulfate areas of Yellowstone and is well correlated to shallow soil temperatures. The extrapolation of diffuse CO₂ fluxes across all the thermal/ altered area suggests that 410 ± 140 t d⁻¹ CO₂ are emitted at HSB (vent emissions not included). Diffuse fluxes of H₂S were measured in Yellowstone for the first time and likely exceed 2.4 t d⁻¹ at HSB. Comparing estimates of the total estimated diffuse H₂S emission to the amount of sulfur as SO₄²⁻ in streams indicates ~50% of the original H₂S in the gas emission is lost into shallow groundwater, precipitated as native sulfur, or vented through fumaroles. We estimate the heat output of HSB as ~140–370 MW using CO₂ as a tracer for steam condensate, but not including the contribution from fumaroles and hydrothermal vents. Overall, the diffuse heat and volatile fluxes of HSB are as great as some active volcanoes, but they are a small fraction (1–3% for CO₂, 2–8% for heat) of that estimated for the entire Yellowstone system.

Published by Elsevier B.V.

1. Introduction

The Yellowstone magmatic system has been responsible for three cataclysmic volcanic eruptions over the past 2.1 million years (Christiansen, 2001), and hosts a large hydrothermal system that transmits heat and volatiles to the surface (Fournier, 1989; Lowenstern and Hurwitz, 2008). Manifestations of the hydrothermal system include thousands of active thermal features covering over 60 km² of warm, hydrothermally-altered ground (Yellowstone Center for Resources, unpublished data) and include one of the largest emissions of carbon dioxide (CO₂) from a single magmatic source on Earth (Werner and Brantley, 2003).

Magmatic volatiles at Yellowstone emerge at the ground surface either as dissolved solutes in thermal waters or as gas emitted from pools, fumaroles and soils (Fournier, 1989; Lowenstern and Hurwitz,

2008). Gas emissions at Yellowstone, predominantly CO₂ and hydrogen sulfide (H₂S), are mainly concentrated in active thermal basins that mostly occur within or near the topographic margin of the 640 ka Yellowstone Caldera, or outside the caldera along major structures such as the Norris–Mammoth corridor or the Red Mountain fault zone to the south (Fig. 1). Most of the CO₂ at Yellowstone emerges from acid-sulfate terrains (Werner and Brantley, 2003), which occurs primarily at higher elevations (Fournier, 1989). Also called steam-heated areas, acid sulfate terrains form where geothermal steam and gas condense to form acid pools and clay-altered ground. Acid-sulfate systems are thought to form above vapor-dominated geothermal reservoirs that in turn overlie boiling Cl⁻-rich waters such as those that emerge in Yellowstone's geyser basins (White et al., 1971, Fig. 1).

Most studies of Yellowstone's hydrothermal system have focused on the Cl⁻-rich waters, which emerge from classic liquid-dominated geothermal reservoirs that were extensively explored by a scientific drilling program (White et al., 1971, 1975). Diffuse CO₂ emissions in the liquid-dominated thermal areas were found to be relatively low

* Corresponding author.

E-mail address: cwerner@usgs.gov (C. Werner).

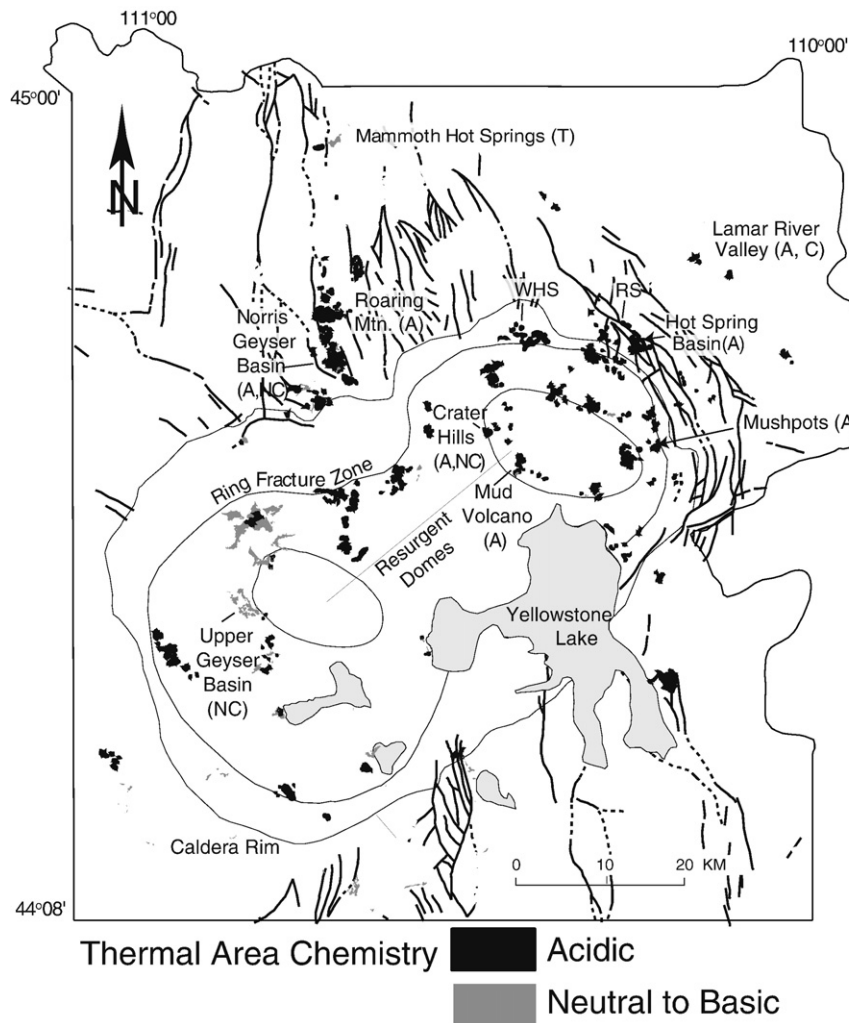


Fig. 1. Map of Yellowstone National Park, Wyoming showing chemical characteristics of fluids from thermal areas (thermal area database courtesy of A. Rodman, Yellowstone National Park). Caldera and resurgent domes from [Christiansen \(2001\)](#). Select thermal areas labeled with descriptor (neutral chloride: NC; acid sulfate: A; travertine: T) Rainbow Springs = (RS), Washburn Hot Springs = (WSH).

compared to CO_2 emissions in the acid-sulfate regions ([Werner and Brantley, 2003](#)). [Werner and Brantley \(2003\)](#) estimated the total diffuse emission from Yellowstone to be $45 \pm 16 \text{ kt d}^{-1}$ of which acid-sulfate regions contributed the majority.

In August 2006, we carried out a study in Hot Spring Basin (HSB), one of the largest acid-sulfate hydrothermal basins in Yellowstone ([Fig. 1](#)). The main objectives of this study were to: 1) characterize and quantify the emission rates of CO_2 and H_2S in vent gases and surface waters; 2) compare emission rates and gas compositions from HSB with other thermally active areas in Yellowstone; and 3) relate HSB emissions to the overall volatile budget of the Yellowstone volcanic system.

2. Geology and field observations

Hot Spring Basin is characterized by numerous areas of acid-altered and thermal ground separated by forested non-thermal areas ([Allen and Day, 1935; Fig. 2](#)). The existing GIS coverage of thermal ground for Yellowstone National Park showed 1.36 km^2 of thermal area at HSB (Yellowstone Center for Resources, unpublished data 2003). However, the coverage included several large expanses of forest and we considered it an overestimate of the actual thermal area. USGS orthophoto quadrangles showed other obvious areas of altered barren ground that were missing from the GIS coverage. We re-

estimated the total area of thermal ground (1.0 km^2) by drawing polygons around bare regions on the relevant orthophoto 90 quadrangles (shown in [Fig. 2a](#)), hypothesizing that such areas are either thermal, or experience a steady flow of acid gas through the soil, thereby resulting in little vegetation. Field observations validated that the barren areas consisted of acid-altered ground typically containing fumaroles, bubbling pools, and mud pots. The largest area of continuous altered ground, the “western basin” (western section of [Allen and Day, 1935](#)), covers $\sim 0.22 \text{ km}^2$ ([Fig. 2b](#)).

The most active thermal feature at HSB is a very loud, slightly superheated ($93.4 \text{ }^\circ\text{C}$) fumarole (YL06-04, [Fig. 2](#)), venting from a wide pit on a non-vegetated slope at the northern end of the western basin ([Fig. 2](#)). Other smaller areas containing active thermal features sampled in this study are herein called upper Shallow Creek, the east basin and the far-east basin, respectively ([Fig. 2](#)). The far-east basin (site of YL06-07) was formed by a large hydrothermal explosion early in the Holocene ([Muffler et al., 1971](#)), but now displays relatively muted hydrothermal activity.

The active thermal features of HSB have developed within the Lava Creek Tuff (LCT) member A ([Christiansen, 2001](#)) and overlying Pinedale-age glacial deposits ([Pierce, 1974; Richmond and Waldrop, 1972; Richmond, 1977](#)) and hydrothermal explosion deposits ([Fig. 2](#)). Glacial deposits consist of gray, massive, varved silt and sandy lake sediments that vary in thickness from $\sim 1.5\text{--}4 \text{ m}$. These overlie

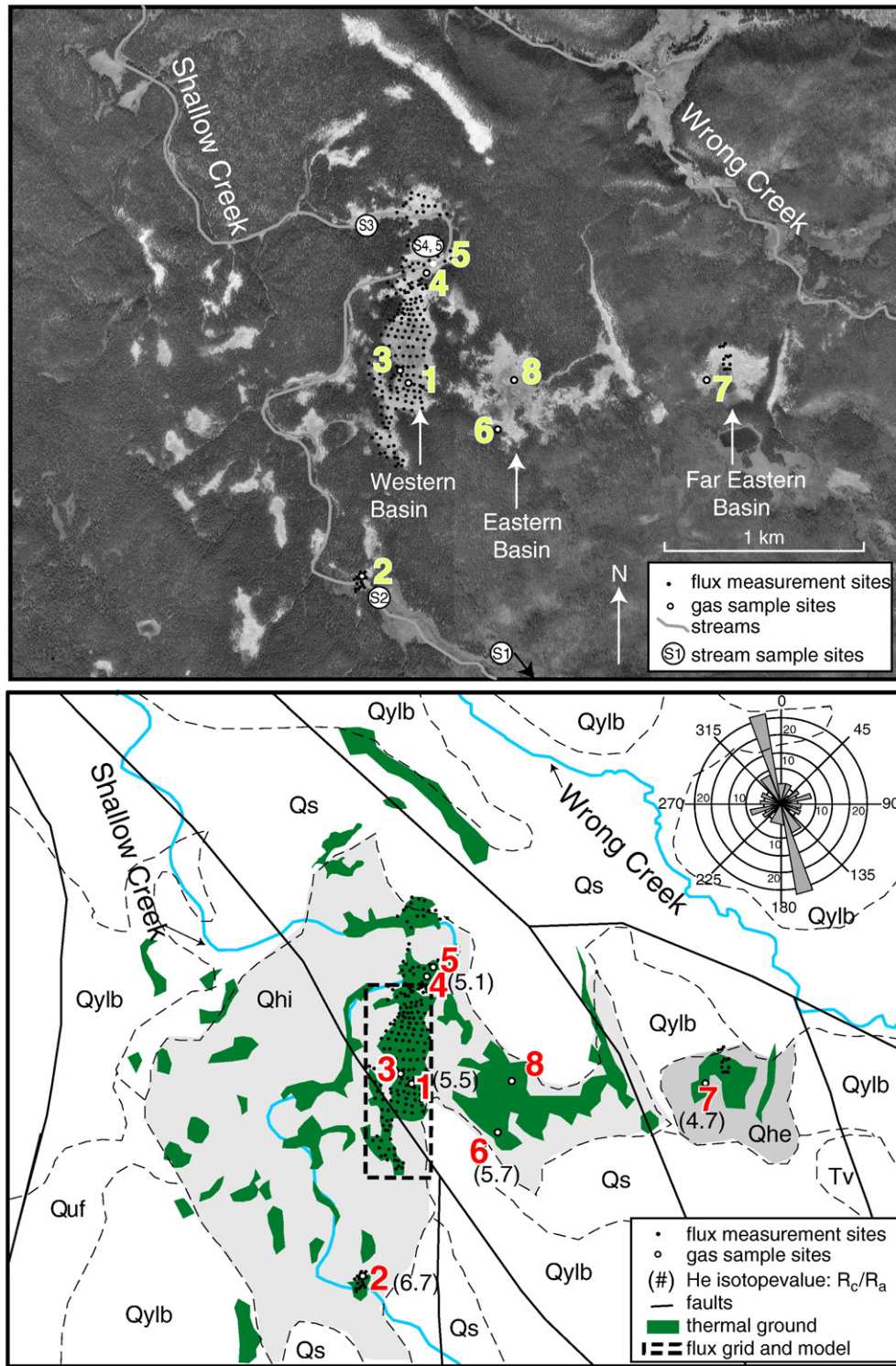


Fig. 2. (a) Rectified orthophoto showing areas of altered ground in Hot Spring Basin (HSB), flux measurement sites, and gas and stream sampling locations. Gas sample sites are shown with numbers and stream sample sites have S prefix before the number. (b) Similar-scaled map showing sample locations, faults, and regions of barren/thermal ground (summing to 1 km², as discussed in text). The dashed rectangle contains the 0.155 km² area of thermal ground where CO₂ flux data were used to estimate the emission rate for the western basin (see Fig. 6 and Table 3). Helium isotope ratios (in parentheses) show an increasing trend to the south. The rose diagram shows the dominant trend of fractures around Hot Spring Basin, primarily within the 640 ky Lava Creek Tuff. Geologic units are as follows: Qylb: Lava Creek Tuff Unit A; Quf: Undine Falls Basalt; Qs: Quaternary Sediments; Tv: Tertiary Basalts; Qhi: Cemented ice-contact deposits; Qhe: Hydrothermal-explosion Deposits (Qhi and Qhe are shaded for easier visualization, all units from Christiansen, 2001).

Pinedale age till and compacted Bull Lake-age clay, silt and sand (up to 50 m thick).

Faults in the area are predominantly normal and trend to the north, northwest, and west-northwest, with some northeast trends within the fractured and welded tuff (Prostka et al., 1975a,b). Preliminary

field measurements, shown as a Rose diagram in Fig. 2b, identified the following structural trends: (1) N and NNW-trending fractures in Lava Creek B outcrops at a hydrothermal-explosion crater in the east (near fumarole sample YL06-07); (2) nearly E–W (111° to 115°) and N–S (010 to 017) fractures in cemented kames; (3) NE fractures (045 to 050)

within the compacted lake sediments exposed in the walls of a large pool; and (4) NW-trending (345) valley (Fig. 2b). The major sub-basins within HSB generally follow the northwest trend of mapped faults (Christiansen, 2001), and faults and fractures also seem to affect the course of both Shallow and Wrong Creeks, which drain HSB.

3. Methods

3.1. Gas collection and analyses

Samples of gas plus steam were collected from fumaroles, bubbling pools and boiling ground (“frying pans”) (Table 1). For fumaroles, a titanium tube was placed in the vent and the area surrounding the tube was packed with mud or soil to ensure good steam and gas flow and minimal air contamination. Pools and frying pans were sampled by means of a partially-submerged funnel that allowed transmission of gas and steam without mixing with air. Both the funnel and titanium tube were fitted with temperature-resistant Tygon tubing to connect it to an evacuated bottle partly filled with a 4 N caustic (NaOH) solution. The length of the tubing varied from 1 to 3 m. Steam and gases such as CO₂ and H₂S were collected in the caustic solution and the more inert gases including H₂, He, N₂, Ar, O₂, CH₄ and other hydrocarbons, were collected in the head space. Sampling terminated when the bottle was full (i.e. when water had condensed such that less than half of the original head space remained). At some sites samples for noble-gas isotope analyses were collected using a ~30-cm length of copper tubing. While gas flowed through the tubing, the ends were sealed using refrigeration clamps to achieve a leak-tight metal seal. More information on collection methods are available in Giggenbach and Goguel (1989) and Fahlquist and Janik (1992).

Constituents of the head space were measured by gas chromatography with a Varian CP-3800 equipped with dual thermal-con-

ductivity detectors and a flame ionization detector. Gases dissolved within the NaOH solution were measured by manometry (CO₂), ion chromatography (Cl⁻, F⁻ and H₂S, after its oxidation to form SO₄²⁻) and gas-sensing electrode (NH₃) at the USGS volcano gas geochemistry laboratory in Menlo Park, California, according to procedures outlined in Fahlquist and Janik (1992) and Evans et al. (2002). CO₂ for carbon isotope analysis was extracted from an aliquot of the caustic solution on a vacuum extraction line using phosphoric acid, following the standard procedure of McCrea (1950). Carbon isotope values were determined on a Finnigan Mat dual inlet mass spectrometer, at the USGS stable isotope laboratory in Menlo Park, CA.

Helium, neon and argon isotopes were measured at the USGS Noble Gas Laboratory in Denver, CO. Bulk gas samples were expanded into an ultra-low vacuum extraction line and the reactable gases were removed using a trap containing STS-707 pellets at 623 K. The remaining gases were exposed to a charcoal trap at 77 K then a cryogenic trap at 11 K, separating the argon fraction from the helium and neon fractions. The charcoal trap was then isolated and heated to approximately 450 K, releasing the Ar component, which in turn was analyzed on a quadrupole mass spectrometer run in static mode. The helium and neon isotopes were separated by incremental heating of the cryogenic trap and analyzed each on a MAP-215-50.

3.2. Diffuse soil CO₂ and H₂S gas flux

Soil gas fluxes of CO₂ and H₂S were measured using West Systems[®] flux meters equipped with accumulation chambers. Accumulation chamber measurement techniques and flux-calculation methods have been described by Chiodini et al. (1998) and Werner et al. (2000). The two instruments used in this study, were outfitted with a LICOR 820 infrared CO₂ gas analyzer (maximum concentration 20,000 ppm), and one instrument also utilized a Dräger Polytron II electrochemical H₂S

Table 1
Gas geochemistry of samples from Hot Spring Basin (species in mol%)

Sample	YL06-01	YL06-02	YL06-03	YL06-04	YL06-05	YL06-06	YL06-07	YL06-08
Date	08/28/06	08/29/06	08/29/06	08/29/06	08/29/06	08/30/06	08/30/06	08/30/06
Type	Fum	Fry	Fry	Fum	Pool	Fry	Fum	Pool
Easting	0558800	0558553	0558752	0558890	0558925	0559263	0560345	0559347
Northing	4954767	4953761	4954838	4955349	4955398	4954529	4954787	4954788
Temp (°C)	91.9	91.9	91.4	93.4	76.9	90.1	90.9	68.1
Basin	Western	usc	Western	Western	Western	East	Far-east	East
X _g (%)	1.4%	81.8%	2.4%	3.7%	88.1%	0.7%	0.7%	97.2%
CO ₂	93.17	94.03	89.99	90.66	91.13	91.22	92.09	94.73
H ₂ S	2.33	3.35	2.08	1.82	1.76	3.09	4.31	3.54
NH ₃	0.003	0.000	0.006	0.146	0.000	0.749	0.006	0.000
He	0.0080	0.0056	0.0083	0.0079	0.0090	0.0045	0.0029	0.0018
H ₂	3.526	1.337	6.969	5.764	3.984	4.362	0.049	0.065
Ar	0.0051	0.0124	0.0050	0.0041	0.0365	0.0061	0.0296	0.0166
O ₂	0.007	0.003	0.010	0.004	0.010	–	0.004	0.001
N ₂	0.171	0.477	0.155	0.103	1.476	0.204	2.324	0.642
CH ₄	0.768	0.768	0.758	1.449	1.536	0.361	1.148	0.958
C ₂ H ₆	0.016	0.011	0.015	0.046	0.048	0.010	0.027	0.036
C ₃ H ₈	0.0023	0.0010	0.0027	0.0118	0.0122	0.0009	0.0063	0.0102
C ₄ H ₁₀	–	–	–	0.0101	0.0105	–	0.0054	0.0088
HCl	–	0.002	–	0.0010	0.0050	–	0.0140	0.0130
HF	–	–	–	–	–	–	–	–
δ ¹³ C _{CO2}	–5.0	–4.0	–4.9	–4.3	–4.6	–5.4	–5.3	–5.5
CO ₂ /H ₂ S	40.0	28.0	43.2	49.9	51.7	29.6	21.4	26.8
CO ₂ /H ₂ S _w	51.6	36.2	55.7	64.4	66.7	38.1	27.6	34.5
R _C /R _A	5.52	6.73	–	5.10	–	5.67	4.71	–
⁴⁰ Ar/ ³⁶ Ar	418	367	–	466	–	369	287	–
N ₂ /Ar	33.7	38.6	30.8	25.2	40.4	33.3	78.5	38.7

usc = Upper Shallow Creek.

X_g is mol% all gases relative to gas plus steam.

Fum = fumarole, Fry = frying pan or boiling ground, Pool = bubbling pool.

–: below detection limit; CO₂/H₂S_w = weight ratio.

R_C/R_A: Air-corrected ³He/⁴He (sample)/³He/⁴He (air).

Locations are in UTM North American Datum 83, Zone 12T.

gas analyzer (maximum concentration 25 ppm, see below). The configuration of LICOR analyzers and chamber sizes allowed us to measure CO₂ fluxes between 2 and 32,000 g m⁻² d⁻¹. The Dräger-chamber configuration allowed for a lower detection limit of 1.7 g m⁻² d⁻¹ H₂S and a variable maximum flux, due to loss of analyzer linearity at H₂S concentrations greater than 20 ppm. The maximum flux measurable is dependent on both the gas concentration and the degassing rate. For a measurement that obtains the 20 ppm H₂S limit over a 20–30 second interval, a conservative estimate of the maximum H₂S flux would be around 17 g m⁻² d⁻¹. However, if the 20 ppm limit is reached over 10 s, the maximum H₂S flux that could be measured would be ~47 g m⁻² d⁻¹. Fluxes greater than this value could still be recorded, as the analyzer can detect up to 25 ppm H₂S, but the nonlinear response of the analyzer over 20 ppm will result in underestimation of the flux (G. Virgili, WEST Systems®, personal communication, 2006).

A total of 228 CO₂ flux and soil temperature measurements were carried out across HSB, with the majority (*n*=160) located in the western basin (Fig. 2). Measurement spacing averaged between 25 and 50 m in the western basin, and 10 to 20 m in the upper Shallow Creek area. Soil temperatures were measured at 10-cm depth at all flux measurement sites. H₂S fluxes were measured only in the western basin and in the upper Shallow Creek area, near fumarole YL06-02. H₂S fluxes were above the detection limit of the analyzer at only 20 sites.

CO₂ fluxes and soil temperatures from the western basin were analyzed using the sequential Gaussian simulation (sGs) algorithm by the program *sgsim* within the geostatistical software GSLIB (Deutsch and Journel, 1998). Details of the application of sGs simulations to CO₂ flux data have been described in detail by Cardellini et al. (2003) and Lewicki et al. (2005). Simulations were performed using a 5-m grid spacing over 0.155 km², the area covered by the flux measurements in

the western basin (Fig. 2). A normal-score data transformation was performed and an experimental variogram was computed and modeled. The variogram model was then used in the sGs procedure to create 1000 realizations of the CO₂ flux and soil temperature across the grid area. Post-processing of the multiple realizations in GSLIB included computation of the mean soil temperature and flux, determination of the 95% confidence interval for the flux mean, and computation of the probability that the flux would exceed 60 g m⁻² d⁻¹ at each grid node. The mean emission rate, in metric tons per day (t d⁻¹) was calculated by summing the simulated fluxes across the grid and multiplying by the area (0.155 km²).

3.3. Water chemistry

Two water samples were collected from Shallow Creek at locations upstream and downstream of HSB and three samples were collected from bubbling pools within HSB. At each sampling site we measured temperature with a thermocouple and digital thermometer and pH using a calibrated meter. Water samples were filtered through a 0.45-μm filter and stored in prerinsed plastic bottles. When needed, samples for cation analyses were preserved by drop-wise addition of high-purity nitric acid to a pH less than 2. Chemical analyses were performed at the USGS in Menlo Park, California. Anion and cation concentrations were determined with a Dionex ICS-2000 ion chromatograph and a Perkin Elmer ELAN 6000 inductively coupled plasma mass spectrometer, respectively. Ammonia concentrations were determined by ion-specific electrode. Analytical uncertainties for all species are ~5%.

Creek discharge measurements were made using the float method (Sanders, 1998) in the major tributary flowing into Shallow Creek above HSB and in Shallow Creek at the downstream end of the western basin. The estimated error in discharge measurements is ±25%.

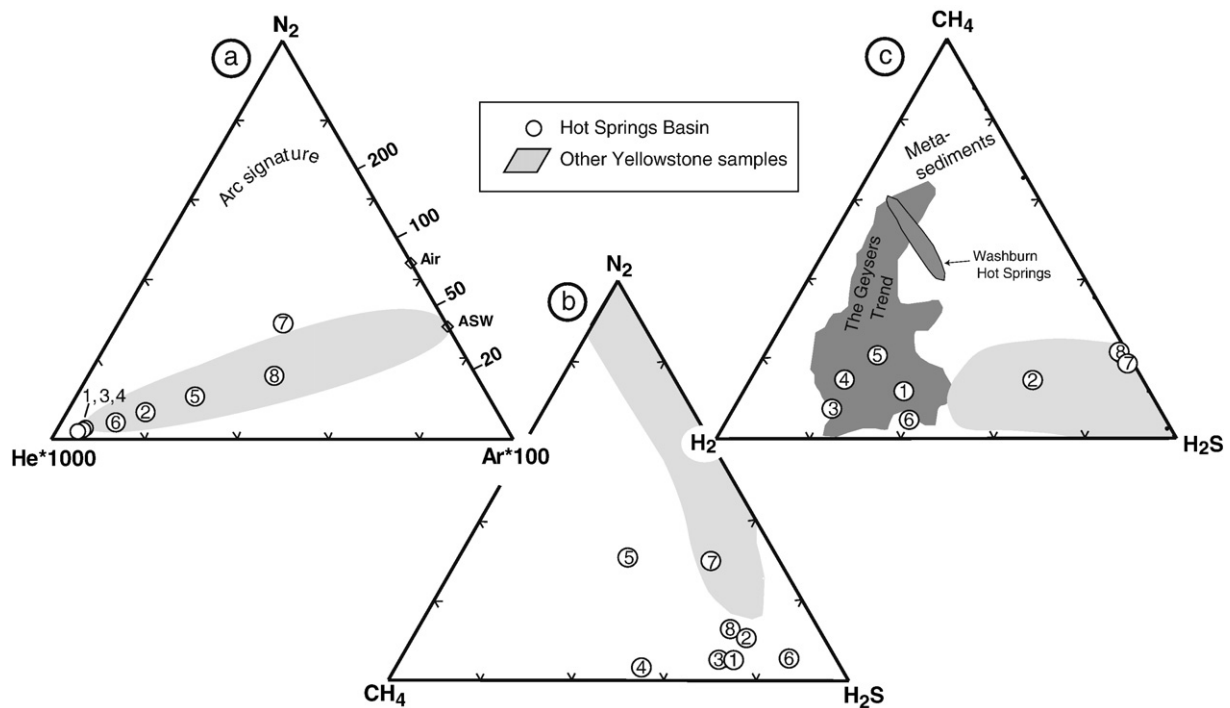


Fig. 3. Ternary diagrams illustrating gas chemistry of thermal features from Hot Spring Basin, compared with other locations at Yellowstone (J. Lowenstern and Deborah Bergfeld, USGS, unpublished data). (a) N₂-100*Ar-1000*He: samples from HSB extend away from a meteoric-water-influenced end member to some of the most He-rich gases found at Yellowstone. (b) N₂-H₂S-CH₄: tendency of HSB gas to be more sulfur-rich than other regions of the park and are CH₄-rich for Yellowstone. (c) CH₄-H₂S-H₂: HSB gases are H₂-rich compared with most areas at Yellowstone, and show much less thermogenic sedimentary influence than found nearby at Washburn Hot Springs (Burnett, 2004) or at areas such as The Geysers, California (Lowenstern and Janik, 2003).

4. Results

4.1. Gas chemistry

Gas samples from boiling-temperature fumaroles and frying pans were dominated by H₂O (between 96.3 and 99.3 mol%), with samples from lower temperature pools containing less H₂O, as expected. On a steam-free basis, all gases contained $\geq 90\%$ CO₂, with smaller amounts of H₂S, H₂, and CH₄ (Table 1). Among the highly soluble gases, NH₃ had a large range in concentration, and HCl and HF were very low and below detection, respectively. Carbon isotope values of CO₂ ranged from -5.5 to -4.0% , and ³He/⁴He ratios ranged from 4.71 to 6.73 times the atmospheric value, R_A , nearly identical to the range of 4.80 to 6.81 R_A reported by Kennedy et al. (1985) for HSB gases collected in 1983.

HSB gases are relatively enriched in He, especially gas from fumaroles YL06-01, -03, and -04, compared with gas from other areas in Yellowstone (Fig. 3a). HSB gases are also among the most sulfur-rich gases at Yellowstone. In the CH₄-H₂S-N₂ system, only one sample from HSB (YL06-07) fell within the range of other Yellowstone samples (Fig. 3b). While HSB samples are CH₄-rich compared to Mud Volcano (Werner and Brantley, 2003), they are not particularly so when compared to other thermal areas in the northeastern part of Yellowstone. Samples from Washburn Hot Springs (Fig. 3c) and Rainbow Springs have greater concentrations of CH₄, and NH₃ (Burnett, 2004). Many of the samples (i.e., YL06-01, -03, -04, -05, and -06) had higher H₂ concentrations than other samples from Yellowstone (Fig. 3c). In summary, the HSB gases are relatively rich in He, H₂S and H₂, and have somewhat elevated CH₄ relative to other areas in Yellowstone.

Comparison of the gas compositions of features across different parts of HSB shows notable spatial variations in chemistry. For example, relative to CO₂, gases in the western basin were on average more enriched in H₂ and lower in H₂S than gases from the other thermal areas (Fig. 4). The distinct nature of the western basin gases holds true for practically every measured component, regardless of the feature-type (e.g. fumarole vs. frying pan).

4.2. Diffuse soil gas flux

4.2.1. CO₂ flux in the western basin

Diffuse CO₂ fluxes ranged from 2 to $\sim 14,000$ g m⁻² d⁻¹ and soil temperatures at a depth of 10 cm from 9.0 to 93.2 °C (the boiling point of H₂O at 2570 m is about 92 °C). The logarithm of the CO₂ flux values displays a broad positive correlation with soil temperatures at 10-cm-depths (Fig. 5a), similar to that for Mud Volcano, another acid-sulfate

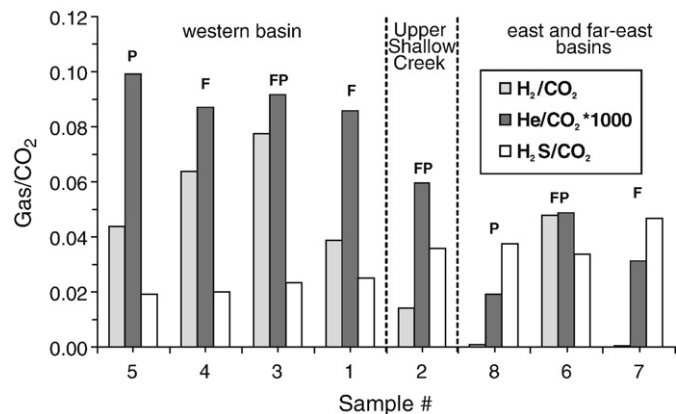


Fig. 4. Comparison of the gas composition across the HSB area showing differences in gases from the western basin as compared with gases in the south and east. Sample numbers (YL06-#) are shown along the X axis. Sample type is indicated by P (Pool), fumarole (F) and frying pan (FP).

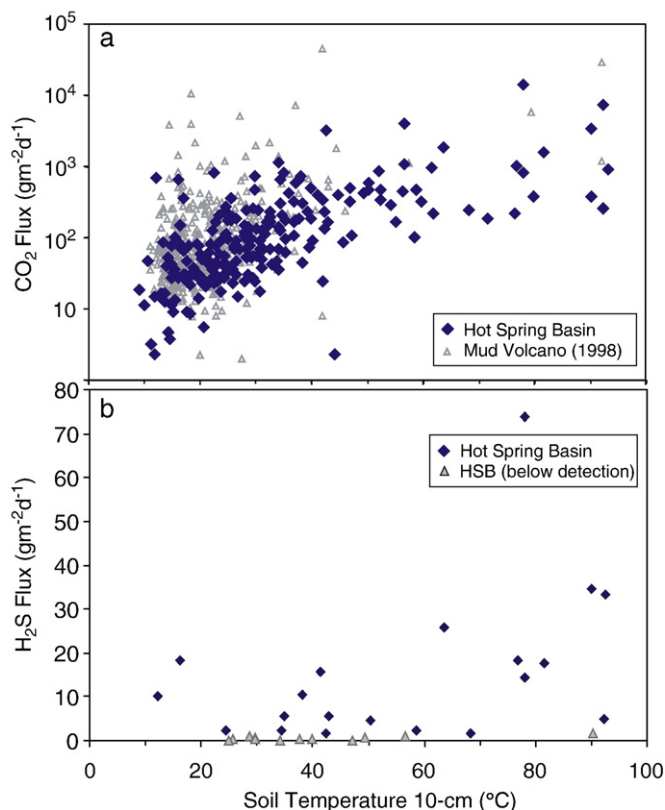


Fig. 5. (a) Broad positive trend in log CO₂ flux and soil temperatures at 10-cm depth for HSB sites compared with data from Mud Volcano (unpublished data from C. Werner (1998)). (b) General positive trend in H₂S flux and soil temperatures at 10-cm depth at 20 sites at HSB.

thermal area at Yellowstone (Mud Volcano data collected in 1998 using similar techniques). At locations with soil temperatures > 70 °C, CO₂ fluxes were between 200 and 14,000 g m⁻² d⁻¹ and at locations with soil temperatures < 20 °C, CO₂ fluxes ranged between 2 and ~ 700 g m⁻² d⁻¹.

Fig. 6a shows the highest fluxes were measured in the middle part of the western basin. The probability map in Fig. 6b displays a good match with the estimated flux map; lower probabilities of high flux (> 60 g m⁻² d⁻¹) were observed along the edges of the western basin whereas higher probabilities of high flux were observed in the middle. The most elevated values on the CO₂ flux map (1000–10,000 g m⁻² d⁻¹) of the western basin (Fig. 6a) are consistent with the highest soil-temperatures mapped for the same region (Fig. 6c), and also with thermal infrared imaging of the western basin and the whole region of HSB (Dr. C. Neale, Utah State University, personal communication April 2008), which shows that the majority of the non-vegetated and acid-altered areas are also areas of hot ground.

The mean CO₂ flux for the western basin data (70% of the basin) was 390 ± 116 g m⁻² d⁻¹ and the mean of all flux data for HSB was 320 ± 74 g m⁻² d⁻¹. The mean emission rate was 63 t d⁻¹ for the modeled area in the western basin (0.155 km²) with a 95% confidence interval ranging from 44 to 85 t d⁻¹. Extrapolating the mean emission rate per unit area (410 t km⁻² d⁻¹) in the western basin to the entire region of altered ground at HSB (1.0 km²) results in total CO₂ emission of 410 ± 140 t d⁻¹. These estimates represent only the diffuse component of the flux and do not account for contributions from fumaroles and bubbling pools; thus, total emissions from HSB would be larger.

4.2.2. H₂S and CO₂ flux relations

H₂S fluxes in the two studied areas ranged from below detection to 74 g m⁻² d⁻¹. In the upper Shallow Creek area measurable H₂S fluxes

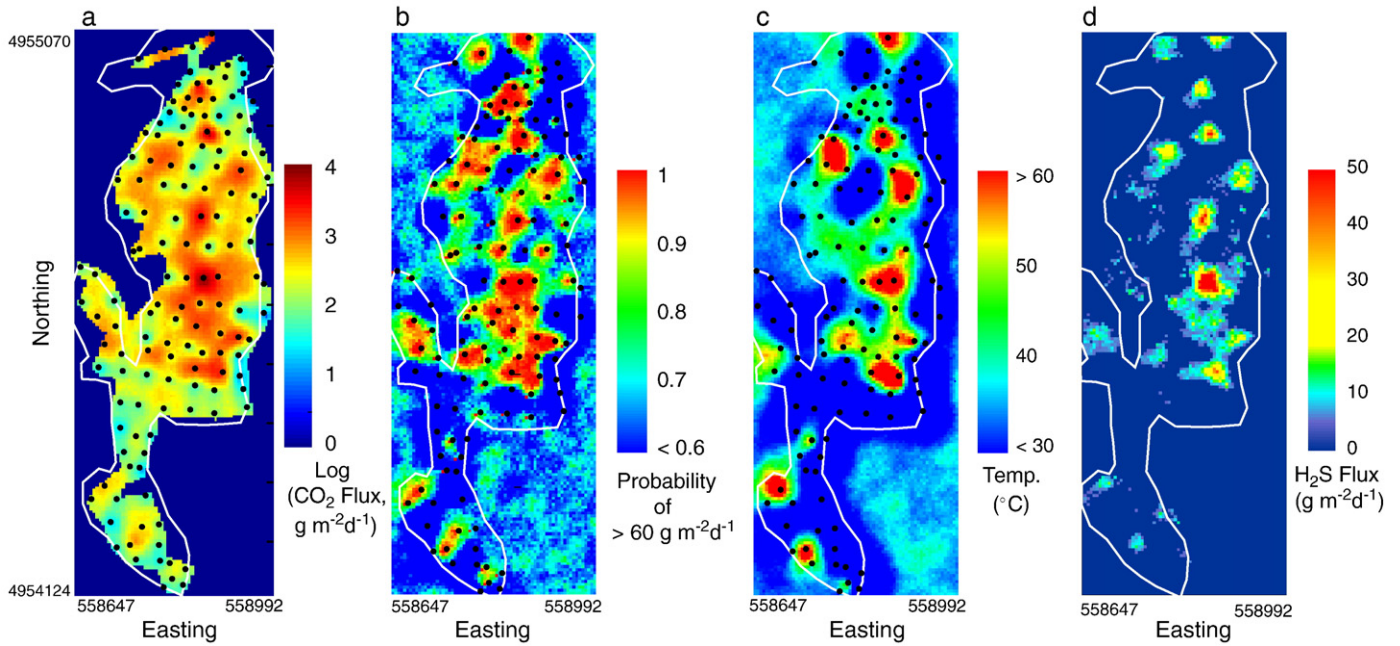


Fig. 6. Maps of sGs results for CO₂ flux, soil temperature and H₂S flux for the modeled part (0.155 km²) of the western basin (Fig. 2b). The white outline shows the extent of thermal area in this region. Small black dots indicate the measurement locations. (a) Simulation results for the CO₂ flux data: blue area was not used for determination of average flux. (b) Map of probability of elevated (> 60 g m⁻² d⁻¹) CO₂ flux over the entire modeled area. (c) Map of the modeled soil temperature distribution at 10-cm depth for the same area in (b) and (d) Map of the H₂S flux estimated from the modeled mean CO₂ flux (Section 4.2). (For interpretation of the references to color in this figure legend, the reader is referred to the web version of this article.)

were recorded at 6 of the 20 investigated sites and in the western basin H₂S fluxes were recorded at 14 of 141 sites (Fig. 7). An additional 12 sites, 11 from the western basin, had an identifiable H₂S flux, but rates were below the detection limit of the analyzer. Relations between CO₂ and H₂S fluxes from the upper Shallow Creek and western basin sites show a strong positive correlation ($r^2=0.9$ and 0.7 , respectively), but with a higher percentage of sites having a detectable H₂S flux in the upper Shallow Creek sites (Fig. 7). Note, however, that this region was also sampled with a smaller spacing. The average mass ratio for the CO₂/H₂S flux for all the HSB sites is about 104 and overall, the flux data from both areas compare fairly well with the range in the mass ratios of CO₂ and H₂S in the gas samples (Table 1, Fig. 7). It is notable that the slightly lower flux ratios at the upper Shallow Creek sites are consistent with the variations in gas chemistry, as the CO₂/H₂S concentration ratio in the gas from the fumarole at the upper

Shallow Creek site is lower than what is found in the gas collected from frying pans and fumaroles in the western basin (Table 1). It is also notable that no appreciable H₂S flux was detected for low CO₂ flux sites; the positive correlation between CO₂ and H₂S fluxes was only observed for sites with CO₂ flux that was greater than a range of flux from ~250–500 g m⁻² d⁻¹. Applying the CO₂/H₂S diffuse flux ratio (104) to the CO₂ fluxes estimated from sgsim modeling that were over this range allowed extrapolation of H₂S flux over the western basin (Fig. 6d). Following from that, the H₂S flux map differs from the CO₂ flux map in that appreciable H₂S is very localized within the central part of the basin. The maximum H₂S flux predicted from the modeled data was ~130 g m⁻² d⁻¹, and the mean emission was calculated as 0.5–0.65 t d⁻¹ depending on whether the low (250 g m⁻² d⁻¹ CO₂) or high (500 g m⁻² d⁻¹ CO₂) threshold was used.

4.3. Water chemistry and solute fluxes

Water-chemistry data was previously published (Hurwitz et al., 2007b), but the relevant results are given here for clarity. The waters flowing into HSB from Shallow Creek had a pH=7.2 at 4.3 °C, whereas the waters at Shallow Creek below the basin were acidic and much warmer (pH=2.4 and $T=27.2$ °C). Downstream waters were enriched in all cations and anions relative to upstream samples. The bubbling pools in HSB were characterized by variable and acid pH values (2.5–5.3), high temperatures (87.7–91.0 °C), high SO₄²⁻ (>649 mg L⁻¹), low Cl⁻ (<1 mg L⁻¹), and relatively high NH₄⁺ (77 to 231 mg L⁻¹). Alkalinity was not measured as the pH of all samples was low except for the upstream sample of Shallow Creek. Thus it was assumed that no HCO₃⁻ was present in appreciable quantities in the water leaving the basin. The calculated water discharge from the western basin of HSB (55 L s⁻¹) was determined from the difference in the flow of Shallow Creek above and below the basin. Related solute fluxes were calculated as 3086 and 3.1 kg d⁻¹ for SO₄²⁻ and Cl⁻, respectively (the SO₄²⁻ discharge converts to 1.1 t d⁻¹ H₂S for Shallow Creek in Table 3). Dividing the SO₄²⁻ discharge by the thermal area drained by Shallow Creek above our sampling point (0.54 km²) gives an average SO₄²⁻ flux of 5.5 g m⁻² d⁻¹.

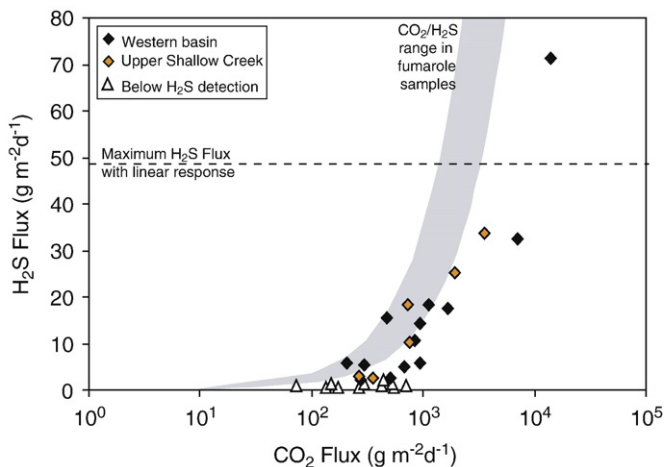


Fig. 7. H₂S vs. CO₂ flux across HSB. In the western basin, diffuse flux ratios are similar to the ratios of the concentrations of H₂S and CO₂ in the fumaroles, or have slightly higher CO₂/H₂S.

5. Discussion

Hot Spring Basin lies just outside the caldera rim, along a series of faults associated with the Mirror Plateau Fault Zone (Christiansen, 2001). As increased hydrothermal flux is often observed aligned with or controlled by geologic structures (e.g., Werner and Cardellini, 2006, and references therein), this location makes HSB a preferred region for gas-rich hydrothermal upflow and likely explains the large extent and preferred orientation of thermal acid-altered areas. HSB is one of the largest hydrothermal areas at Yellowstone and is associated with a negative gravity anomaly and *P* and *S* seismic velocity lows that are likely related to a large vapor- or liquid-saturated region at depth (Lehman et al., 1982; Miller and Smith, 1999).

The diverse dataset presented here suggests that the ascent of magma-derived volatiles to the ground surface is complex. Nevertheless, the composition of the volatiles at HSB is typical of vapor-dominated systems (White et al., 1971) with abundant emissions of gaseous CO₂, and H₂S, some of the latter converted to dissolved SO₄, and precipitated native sulfur. Discharge of Cl⁻ and F⁻ is minor, but dissolved NH₄⁺ is elevated in surface waters.

5.1. Volatile sources

Compared to other regions of Yellowstone, HSB gases are notably He-rich. Most samples had between 0.005 and 0.009 mol% He, whereas gas from many other areas in Yellowstone typically contain <0.005 mol% He. Samples plotting near the helium apex of the ternary diagram (Fig. 3a) are commonly thought to be heavily influenced either by magmatic He input or input of crustal He produced through alpha-decay of U–Th series elements (Giggenbach, 1996). ³He/⁴He ratios in HSB gas are not especially high ($R_C/R_A=4.71$ – 6.73), especially when compared to Mud Volcano, the area with the strongest mantle signature (e.g., $R_C/R_A=16$ – 17 , Kennedy et al., 1985; Werner and Brantley, 2003). Thus, the relatively low R_C/R_A and high He concentration indicate a substantial component of crustal He is added to HSB gas compared to areas such as Mud Volcano, Norris Geyser Basin, or Crater Hills that have relatively less He but a higher mantle helium content (Kennedy et al., 1985; A. Hunt, J. Lowenstern, D. Bergfeld, unpublished data, 2003–2007).

With CH₄ concentrations as high as 1.5 mol%, gas from HSB shows some contribution from a sedimentary source. The sedimentary signature at HSB is weaker than that seen in gas from nearby Rainbow Springs and Washburn Hot Springs, which have CH₄ concentrations as high as 2–8 mol% (Clifton et al., 1990; Burnett, 2004). Those areas are located near the northeastern caldera boundary, and have long been recognized as having hydrocarbon-rich gases derived from breakdown of sedimentary materials (Love and Good, 1970; Clifton et al., 1990). However, when compared with Mud Volcano which lies inside the caldera, some sedimentary signature at HSB is apparent and is evidenced both by relatively higher CH₄ concentrations (Fig. 3b and c) and relatively lower $\delta^{13}\text{C-CO}_2$ values, which range from to -5.5 to -4.0% , and -4.8 to -3.2% , respectively (Table 1; J. Lowenstern and D. Bergfeld, unpublished data). CH₄ abundances at HSB were similar to the Mushpots thermal area, which lies several kilometers to the south (Fig. 1). Finally, HSB gases are not particularly CH₄-rich when compared with other geothermal systems with a strong sedimentary component such as The Geysers, California (Fig. 3c, Lowenstern and Janik, 2003).

A limited sedimentary signature at HSB is also supported by NH₃ concentrations in gases and the NH₄⁺ contents of thermal waters. In regions heavily influenced by sedimentary sources, NH₃ concentrations can be quite high, sometimes exceeding H₂S (Fournier, 1989). Similarly, high NH₄⁺ concentrations are found in thermal waters such as at Washburn Hot Springs where concentrations of 650 mg L⁻¹ have been reported (McCleskey et al., 2005). Our findings show that NH₃ in the gas at HSB was 1–3 orders of magnitude less than H₂S and

Table 2

Solute concentrations (mg/L) and molar ratios in samples from Shallow Creek (bold) and bubbling pools

	SH01	SH02	SH03	SH04	SH05
Easting	0559524	0558543		0558905	0558868
Northing	4953203	4953753	–	4955419	4955389
<i>T</i> (°C)	5.3	89.2	27.2	87.7	91.0
pH	7.2	5.2	2.5	3.1	2.5
Na	3.0	1.6	19	130	31
K	2.1	3.8	19	227	64
Ca	3.4	0.5	7.2	19	4.4
Mg	1.8	0.2	2.1	4.2	1.7
Fe	<0.2	<0.2	2.9	12.3	4.9
Al	<0.1	0.2	17	2.1	18
SiO ₂	36	178	148	288	282
Cl ⁻	0.4	0.7	0.6	1.7	0.5
SO ₄ ²⁻	4.3	649	550	1304	1104
HCO ₃ ⁻	24	–	–	–	–
F	0.3	0.4	0.5	0.6	0.4
NH ₄ ⁺	<1	230	15	165	77
Mg/Ca	0.9	0.5	0.5	0.4	0.6
Na/K	2.4	0.7	1.7	1.0	0.8

the maximum concentration of NH₄⁺ in the waters was 230 mg L⁻¹ (Tables 1 and 2).

5.2. Reservoir temperatures

Numerous gas geothermometers have been developed and applied to fumarole and hot spring gases, but none are considered reliable in all cases. The empirical gas geothermometer of D'Amore and Panichi (1980) assumes that the relative concentrations of H₂, CH₄, H₂S, and CO₂ are controlled by reservoir temperature; e.g., that any sediment-derived CH₄ has re-equilibrated with other gases and mineral buffers. An additional assumption is that near-surface processes such as preferential dissolution of highly soluble H₂S or CO₂ into shallow groundwater are insignificant. These assumptions are supported here by the fairly small enrichment in CH₄ (Fig. 3b and c) and low relative abundance of Ar and N₂ (Fig. 3a) that would be increased by interaction with shallow groundwater. Based on the D'Amore and Panichi geothermometry, calculated equilibration temperatures for the HSB samples are 230–300 °C and average 268 °C. This compares to ~140–180 °C at Mud Volcano, ~200 °C at the Mushpots, and ~220 °C at Norris calculated by Goff and Janik (2002) using the same geothermometer. The H₂/Ar geothermometer of Giggenbach et al. (1994) gives an average temperature of 329 °C for HSB, while the CH₄–C₂H₆–C₃H₈ geothermometer of Tassi et al. (2007) gives an average temperature of 233 °C, bracketing the D'Amore and Panichi (1980) result.

The high calculated temperatures for HSB gases are consistent with the geophysical indications that the northeastern region of the caldera hosts a highly-fractured fluid-filled area overlying some of the shallowest partial melt in Yellowstone (Smith and Braile, 1994; Miller and Smith, 1999). The temperatures are also consistent with the hypothesized 330–350 °C, deep 'parent' fluid underlying the Yellowstone Caldera, determined from enthalpy–chloride relationships from various geyser basins in western regions (Truesdell and Fournier, 1976; Fournier, 1989). At Hot Spring Basin, the lack of high-Cl fluid outflow suggests that parent fluid does not approach the surface, but instead boils at depth, producing the steam, CO₂, H₂S and other gases that emerge in this acid-altered terrain.

5.3. Spatial variations

The variability in gas chemistry across HSB probably reflects, at least in part, spatial variations within the deep hydrothermal reservoir (s) that feed(s) the surface features. Reservoir heterogeneities are seemingly required to explain the significant range in ³He/⁴He ratios,

4.71–6.73 R_A (Table 1) and 4.80–6.81 R_A found in 1983 by Kennedy et al. (1985; values provided by B.M. Kennedy, Lawrence Berkeley Laboratory, written communication Feb. 28, 2008). For samples as enriched in total helium as the HSB suite (Table 1; Fig. 3a), processes such as radiogenic ingrowth are too slow to alter the $^3\text{He}/^4\text{He}$ ratios during upflow of gas and steam to the surface. Interestingly, the four sites sampled in 1983 form a N–S transect comparable to our samples YL06-04, -01, -02 and show the same southward increase in $^3\text{He}/^4\text{He}$ ratios. The distance over which the increase occurs (1–2 km, Fig. 2) is consistent with a gradient at reservoir depths.

The spatial variability observed in HSB gas chemistry strongly suggests a solubility-based control on gas chemistry. Samples with high H_2/CO_2 and high He/CO_2 ratios, e.g., western basin samples, also have low $\text{H}_2\text{S}/\text{CO}_2$ ratios (Fig. 4). Thus, gas-ratio comparisons across HSB show that enrichment in He and H_2 , gases less soluble than CO_2 , is clearly coupled to depletion in the more soluble H_2S . This behavior was also borne out by variations in the diffuse H_2S to CO_2 flux ratios (Fig. 7). The apparent solubility control on gas chemistry may be due to spatial heterogeneities in deep reservoir boiling where enrichment in the least soluble gases would reflect smaller degrees of boiling. Subsequent preferential loss of more soluble gases such as CO_2 and H_2S into shallow groundwater does not seem to be the major cause for the observed variations. Western basin samples with high He/CO_2 ratios generally show less interaction with shallow groundwater (ASW) in Fig. 3a, and as a group have similar gas ratios despite the fact that one sample is from a slightly superheated fumarole (YL06-04) and another is from a pool of water well below boiling temperature (YL06-05). Thus, near-surface effects on vent-gas chemistry appear to be small, although minor and local microbial modification of H_2 and H_2S cannot be ruled out (Xu et al., 1998).

5.4. Noble gas isotope systematics

Kennedy et al. (1985) found that the helium and argon isotope compositions for all 66 samples collected from 19 different thermal areas fit within an area between magmatic and radiogenic trends on a rare-gas isotope plot (Fig. 8). Air and air-saturated water are indistinguishable in this plot, and form one end-member source common to all samples. The two other end members needed to explain the data array were identified by Kennedy et al. (1985) as magmatic gas, with a $^{40}\text{Ar}/^{36}\text{Ar}$ ratio significantly greater than air, and

crustal gas consisting of radiogenic ^4He and ^{40}Ar but no ^{36}Ar . Gas from Mud Volcano, with the highest $^3\text{He}/^4\text{He}$ ratio in Yellowstone, was considered most representative of the magmatic end member. Other samples, with lower $^3\text{He}/^4\text{He}$ ratios, plotted on lines of progressively lower slopes radiating away from the air end member. The correlation between lower $^3\text{He}/^4\text{He}$ and lower slope allowed Kennedy et al. (1985) to determine that the crustal end member, with an assumed $^3\text{He}/^4\text{He}$ ratio of 0.01 R_A had a radiogenic production ratio of $^{40}\text{Ar}/^4\text{He}$ ($^{40}\text{Ar}/^4\text{He}$) of 0.25 (Fig. 8), which corresponds to a K/U ratio of 14,000 in the reservoir rocks.

The 2006 samples from HSB are noteworthy in that 3 of them plot along the radiogenic component line (Fig. 8), mainly due to an extremely small air component. This shift away from the air end member relative to the 1983 samples most likely reflects decreased involvement of shallow groundwater and possibly drier conditions during sampling in 2006, although increased upflow of deep gases could be an alternate possibility. Regardless, the minor influence of shallow groundwater on gas chemistry discussed earlier is highlighted by results shown in Fig. 8. Even sample YL06-07 is mainly affected by air contamination, not interaction with shallow groundwater, as is shown by its high N_2/Ar ratio (Table 1, Fig. 3a).

Although sample YL06-02 plots among the group of lines radiating from air through the 1983 samples (Fig. 8), YL06-06 plots below any such line, and samples YL06-01 and -04 are distributed slightly below the radiogenic production line of Kennedy et al. (1985). Because all HSB samples have $^3\text{He}/^4\text{He}$ ratios that are $\gg 0.01 R_A$ (Table 1), they must contain a significant component of magmatic He and Ar, so it is clear that the crustal (radiogenic) production ratio of $^{40}\text{Ar}/^4\text{He}$ is substantially less than 0.25 as noted by Kennedy et al. (1985). By assuming that the $^{40}\text{Ar}/^4\text{He}$ and $^3\text{He}/^4\text{He}$ ratios at Mud Volcano represent the magmatic end-member, $^{40}\text{Ar}/^4\text{He}$ ratios can be calculated through

$$^{40}\text{Ar}/^4\text{He} = \left(\left(\frac{^{40}\text{Ar}}{^{36}\text{Ar}} \right)_S - \left(\frac{^{40}\text{Ar}}{^{36}\text{Ar}} \right)_A - 0.7x \right) / \left(\left(\frac{^4\text{He}}{^{36}\text{Ar}} \right)_S - x \right)$$

where $x = (^4\text{He}/^{36}\text{Ar})_S / (^3\text{He}/^4\text{He})_S / (^3\text{He}/^4\text{He})_{MV}$, and subscripts S , A , MV refer to sample, air, and Mud Volcano, respectively. Under this assumption, $^{40}\text{Ar}/^4\text{He}$ ratios for YL06-01, -04, -06 are indistinguishable from zero (-0.03 ± 0.06) and correspond to a K/U ratio of less than 2000 (at a $\text{Th}/\text{U} \leq 5$). This low K/U is incompatible with analyzed samples of the Lava Creek tuff (Christiansen, 2001) or any other primary igneous rocks at Yellowstone, but could be consistent with derivation from limestones and quartz-rich sediments that are presumably deeply buried beneath the Eocene Absaroka volcanics in this area. The need to invoke multiple fluid sources at reservoir depths, as discussed earlier, is thus made clear by the combined helium and argon isotope systematics.

5.5. Soil temperatures and diffuse CO_2 emissions

In the western basin there is a positive correlation between diffuse CO_2 flux and soil temperature, indicating that in general, CO_2 travels with rising steam. The CO_2 -temperature trend for the HSB data is similar to that seen at Mud Volcano in 1998 (Fig. 5a). Of the two, HSB had proportionately more locations with high soil temperatures (40–97 °C) than Mud Volcano, likely because the western basin at HSB has a larger contiguous area of steam and gas output (sample spacing was similar in both studies: ~25–40 m) and because the edges of the thermal area were not well documented at HSB (no measurements were made in vegetated or forested areas). The correlation between soil temperature and flux (Figs. 5a, 6b and c) lends additional support for extrapolation of the CO_2 emissions estimate for the western basin across all of the thermal/ altered area at HSB (Fig. 2), but also suggests that this extrapolated CO_2 emission rate may be low as high CO_2 fluxes are sometimes observed in areas with cooler soils (Fig. 5, see also Werner et al., 2000). Results from

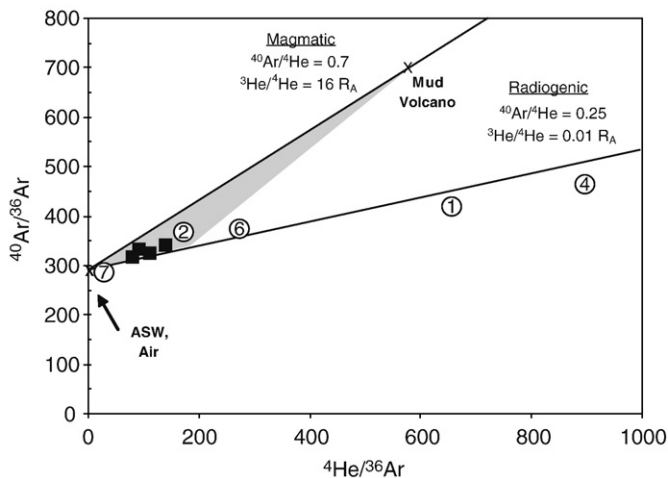


Fig. 8. Plot of $^{40}\text{Ar}/^{36}\text{Ar}$ vs. $^4\text{He}/^{36}\text{Ar}$ for Yellowstone gases. Gray triangular region represents 66 samples collected from 19 thermal areas in the early 1980s, including 1983 HSB samples (filled squares) from Kennedy et al. (1985). Line through Mud Volcano gives minimum slope for magmatic gas end member. “Radiogenic” line calculated by Kennedy et al. (1985) from three-dimensional regression analysis. Filled circles are 2006 HSB samples numbered as in Table 1.

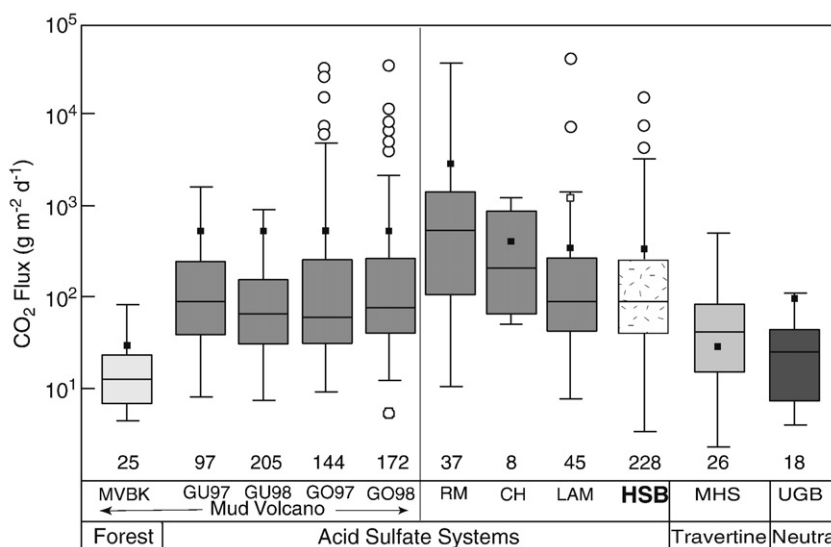


Fig. 9. Box and whisker plot of the CO₂ flux populations in the Mud Volcano area (GU: Gumper region in 1997 and 1998; GO: Goose region in 1997 and 1998; MVBK: background forest), Roaring Mountain (RM), Crater Hills (CH), Lamar Valley cold degassing (LAM), Mammoth Hot Springs (MHS) and the Upper Geyser Basin (UGB). All data from Werner and Brantley (2003). Compared are new data from Hot Spring Basin (HSB). The box indicates the 25th to 75th percentile of CO₂ flux values, the whiskers extend to the 10th and 90th percentiles, and the line in the box represents the median value. The circles represent measurements that fall outside three standard deviations of the mean. Arithmetic averages for the populations are shown by small filled squares; the means shown on the GU and GO distributions are the average of all the flux measurements from the medium strata (thermal altered areas) at Mud Volcano (Werner et al., 2000); see text for more details. The open square on the LAM distribution contains one high flux measurement that skews the average; the filled square does not include that data point. The numbers at the bottom (but above the sample abbreviations) represent the number of flux measurements in the populations plotted.

the measured and modeled fluxes from the western basin indicate that CO₂ fluxes could exceed 1000–10,000 g m⁻² d⁻¹ over an area that is > 150×250 m in dimension (Fig. 6b).

The population distribution, median, and average CO₂ flux for HSB are similar to those measured at Mud Volcano, Crater Hills, and the Lamar River Valley, but lower than those measured at Roaring Mountain (Fig. 9). Our estimate of the areally averaged diffuse CO₂ emission for the 1 km² of altered area at HSB is 410 ± 140 t km⁻² d⁻¹, or about 24% greater than Mud Volcano. Different techniques were used to estimate total CO₂ emissions from Mud Volcano and HSB. At Mud Volcano, Werner et al. (2000) used a stratified adaptive sampling plan for their medium degassing strata (i.e. thermally active acid-sulfate terrain) that yielded an estimate of ~133 t d⁻¹ of CO₂ (1.1 × 10⁹ mol yr; Werner et al., 2000). Based on the 0.4 km² area in that study (Werner et al., 2000) the area average of diffuse CO₂ emission from Mud Volcano was ~330 t km⁻² d⁻¹, lower than the 410 t km⁻² d⁻¹ estimate for HSB. However, the arithmetic average of the individual CO₂ flux measurements from the Mud Volcano medium strata¹ was 540 ± 96 g m⁻² d⁻¹, higher than the arithmetic average of the CO₂ flux measurements at HSB (320 ± 74 g m⁻² d⁻¹). The discrepancy between area averages and arithmetic averages when comparing flux data from HSB and Mud Volcano partly results from the different procedures used to estimate total CO₂ emission rates and highlights some of the uncertainty in the reporting of averages and emission rate estimates from highly skewed and spatially heterogeneous flux data (see also Lewicki et al., 2005). It also signifies that there is not a large difference in the nature of the distribution of CO₂ flux data collected in these two areas of Yellowstone (Fig. 9).

The total diffuse CO₂ emission for HSB is ~1% of that estimated from all thermal areas in Yellowstone (45 ± 16 kt d⁻¹), which was computed using an average value of 1250 g m⁻² d⁻¹ (Werner and Brantley, 2003). This average (1250 g m⁻² d⁻¹ CO₂) included data from

¹ The arithmetic average of the medium strata values used in this paper for Mud Volcano should not be confused with the mean value reported in Table 3 of Werner et al. (2000). The value reported there (1712 g m⁻² d⁻¹) was the mean of the network averages within the medium strata, where a network was a specific component of the sampling design. See Werner et al. (2000) for more details.

higher-flux acid sulfate regions such as Roaring Mountain (see Fig. 9). The diffuse CO₂ emission rate from HSB is comparable to emissions from individual active volcanoes (e.g. Ruapehu or White Island in New Zealand; Werner et al., 2006, 2008).

5.6. H₂S fluxes and the sulfur budget

H₂S is a significant component both in fumarolic and diffuse emanations, SO₄²⁻ is elevated in surface waters, and S-bearing minerals are abundant at the ground surface. The question remains how strongly is, or what proportion of the total S is sequestered into liquid or solid phases at the surface. The general correlation observed between H₂S and CO₂ flux in the western basin allows a first-order estimate of the H₂S diffuse emission rate. For this area, the average fumarole CO₂/H₂S mass ratio was ~60 while the average CO₂/H₂S ratio in the diffuse flux was 104. If the fumarole ratio is characteristic of the deep upflow, then nearly 50% of the H₂S in the diffuse emission is lost, presumably to native sulfur or SO₄²⁻. Using a fumarole ratio of 60 and the total CO₂ emission rate determined above (410 ± 140 t d⁻¹), we would estimate that 6.8 ± 2.3 t d⁻¹ of H₂S is emitted from HSB (Table 3). However, given the CO₂/H₂S diffuse flux ratio measured in the western basin (104), a lower value of ~3.9 ± 1.3 t d⁻¹ H₂S is calculated for the actual diffuse flux. Moreover, this is likely an overestimate given that H₂S

Table 3
Volatile emissions from Hot Spring Basin

	Diffuse CO ₂ (t d ⁻¹)	Expected diffuse H ₂ S (t d ⁻¹)	Measured diffuse H ₂ S (t d ⁻¹)	Dissolved H ₂ S (t d ⁻¹)	Estimated H ₂ O (t d ⁻¹)	Area (km ²)
Western Basin (modeled)	63.5 ± 20	1.0 ± 0.36 ¹	0.5–0.65 ²	–	1000 ⁴	0.155
Shallow Creek drainage	–	–	–	1.1 ³	–	0.55
Total HSB	410 ± 140	6.8 ± 2.3	2.4–3.1	2.0	6450 ⁴	1.0

¹Based on a fumarole CO₂/H₂S weight ratio of 60, ²Based on the measured diffuse CO₂/H₂S weight ratio of 104 and modeled CO₂ flux data in the western basin, ³From Hurwitz et al. (2007a,b) estimates, ⁴Based on the average fumarolic H₂O/CO₂ molar ratio of 39.

was only detected when CO₂ fluxes were greater than ~250 to 500 g m⁻² d⁻¹ (Fig. 7). Applying the diffuse CO₂/H₂S ratio to every grid point in our western basin model over 250 g m⁻² d⁻¹ results in a western basin H₂S emission rate of 0.65 t d⁻¹, or 3.1 t d⁻¹ from HSB (Table 3). Using a stricter cutoff of 500 g m⁻² d⁻¹ CO₂ results in 0.5 t d⁻¹ H₂S from the western basin and 2.4 t d⁻¹ from HSB (Table 3). The difference between the CO₂/H₂S ratio measured in fumaroles vs. diffuse flux values can be explained if some S is dissolved as SO₄²⁻ or precipitated as native sulfur or sulfide and is not emitted. We calculated a flux of ~1.1 t d⁻¹ of SO₄²⁻ in Shallow Creek (which drains 55% of the total 1 km² of thermal area in HSB), suggesting ~2.0 t d⁻¹ of H₂S is converted to SO₄²⁻ for the whole of HSB (Table 3). The remaining 1.7–2.4 t d⁻¹ of H₂S may be expected to be converted to native S or sulfide.

While these estimates represent a good starting point for determining the sulfur budget of a hydrothermal area, there are a number of uncertainties in the above calculations. First, the SO₄²⁻ flux is likely not in steady state and periods of higher precipitation are likely to yield higher solute fluxes (Hurwitz et al., 2007a). Second, more tightly spaced data would be helpful to constrain the relationship between CO₂ and H₂S degassing in high flux areas better.

5.7. Inferences for heat flow

As presented in Chiodini et al. (2001, 2005) the CO₂ flux can be used as a tracer for steam output, and thus for heat flow in hydrothermal areas. This procedure assumes that the H₂O/CO₂ ratio of fumaroles represents the original components and that no condensation has occurred. At Yellowstone, where the fumaroles are at boiling point, there is the possibility that some steam has previously condensed, which adds uncertainty to the estimates. Based on the total diffuse CO₂ emission rate (410 t d⁻¹) and an average CO₂/H₂O molar ratio for western basin fumaroles of 0.026 we calculate ~6450 t d⁻¹ of H₂O flux as steam. At HSB the boiling point of water is 92 °C, corresponding to a steam enthalpy of 2663 J g⁻¹. Multiplying the total steam flux by the enthalpy results in a heat output of about 200 MW. Using the range of fumarole gas/steam (X_g) in the western basin, a heat output between 140 and 370 MW is estimated. The overall heat output from HSB corresponds to between 2 and 8% that for the Yellowstone hydrothermal system (4.5–6 GW) as determined by the Cl-inventory method (Friedman and Norton, 2007). The heat output translates to a heat flux from 140 to 370 W m⁻² for the 1 km² of thermal area at HSB, a value 100 times greater than that for the Yellowstone Caldera as a whole (Fournier, 1989), illustrating that heat loss from the subjacent magma is focused through large thermal areas such as HSB.

6. Conclusions

Gas from HSB is a mixture of magmatic gas with crustal gases rich in He and to a lesser extent CH₄. The spatial variability of the gas geochemistry at HSB likely represents variations in non-magmatic crustal gas sources within the deep hydrothermal reservoir that feeds the surface features. The areally averaged diffuse CO₂ flux at HSB is similar to other acid-sulfate areas at Yellowstone, but because of its large spatial extent, emissions are greater than most other thermal areas in the park. The total diffuse emission of CO₂ at HSB is 410 ± 140 t d⁻¹, similar to some active (but non-erupting) volcanic systems around the world. High gas emissions are consistent with highly fractured terrain and gas-saturated conditions beneath HSB as evident from seismic velocity and gravity lows. Nearly all of the CO₂ is released in gaseous form whereas up to 50% of the sulfur may be oxidized and retained in shallow ground waters and minerals. HSB provides approximately 1% of the estimated diffuse CO₂ emissions at Yellowstone and ~2–8% of the total heat output of the Yellowstone system estimated from Cl⁻ discharge. Future work should utilize these and other techniques to better quantify gas emissions and heat output of

thermal basins distributed around Yellowstone. Only by doing so, can we refine the current estimates of gas and heat discharge from one of Earth's largest active magmatic systems.

Acknowledgements

This study was funded by the U.S. Geological Survey, Volcano Hazards Program. The authors would like to thank the GeoNet program at GNS Science in New Zealand for technical assistance. Mark Huebner processed the gas samples for dissolved anions, and George Hilley of Stanford University assisted with sGs simulations. Mack Kennedy of Lawrence Berkeley National Laboratory provided archive data and helpful discussion of the helium isotope data. Yellowstone National Park provided pack animals and logistical support. This manuscript was improved by the careful reviews of Pat Shanks and Yousif Kharaka and two anonymous reviewers.

References

- Allen, E.T., Day, A.L., 1935. Hot Springs of the Yellowstone National Park, vol. 466. Carnegie Institution of Washington Publication, Washington D.C. 525 pp.
- Burnett, B.J., 2004. Volatile Light Hydrocarbons in Geothermal Gas Emissions from Yellowstone National Park, USGS, and Comparisons to El Salvador and Honduras. M.S. Thesis, University of New Mexico, 95 pp.
- Cardellini, C., Chiodini, G., Frondini, F., 2003. Application of stochastic simulation to CO₂ flux from soil: mapping and quantification of gas release. *J. Geophys. Res.* 108 (B9). doi:10.1029/2002jb002165.
- Chiodini, G., Cioni, R., Guidi, M., Raco, B., Marini, L., 1998. Soil CO₂ flux measurements in volcanic and geothermal areas. *Appl. Geochem.* 13, 543–552.
- Chiodini, G., Frondini, F., Cardellini, C., Granieri, D., Marini, L., Ventura, G., 2001. CO₂ degassing and energy release at Solfatara volcano, Campi Flegrei, Italy. *J. Geophys. Res.* 106, 16213–16222.
- Chiodini, G., Granieri, D., Avino, R., Caliro, S., Costa, A., Werner, C., 2005. Carbon dioxide diffuse degassing and estimation of heat release from volcanic and hydrothermal systems. *J. Geophys. Res.* 110, B08204. doi:10.1029/2004JB003542.
- Christiansen, R.L., 2001. The Quaternary and Pliocene Yellowstone Plateau Volcanic Field of Wyoming, Idaho, and Montana. U.S. Geol. Surv. Prof. Pap., vol. 729-G, p. 144.
- Clifton, C.G., Walters, C.C., Simoneit, B.R.T., 1990. Hydrothermal petroleum from Yellowstone National Park, Wyoming, U.S.A. *Appl. Geochem.* 5, 169–191.
- D'Amore, F., Panichi, C., 1980. Evaluation of deep temperature of hydrothermal systems by a new gas-geothermometer. *Geochim. Cosmochim. Acta* 44, 549–556.
- Deutsch, C.V., Journel, A.G., 1998. GSLIB: Geostatistical Software Library and Users Guide. Oxford Univ. Press, New York. 369 pp.
- Evans, W.C., Sorey, M.L., Cook, A.C., Kennedy, B.M., Shuster, D.L., Colvard, E.M., White, L.D., Huebner, M.A., 2002. Tracing and quantifying magmatic carbon discharge in cold groundwaters: lessons learned from Mammoth Mountain, USA. *J. Volcanol. Geotherm. Res.* 114, 291–312.
- Fahlquist, L., Janik, C., 1992. Procedures for Collecting and Analyzing Gas Samples from Geothermal Systems. U.S. Geological Survey Open-File Report, vol. 92–211. 19 p.
- Fournier, R.O., 1989. Geochemistry and dynamics of the Yellowstone National Park hydrothermal system. *Annu. Rev. Earth Planet. Sci.* 17, 13–53.
- Friedman, I., Norton, D.R., 2007. Is Yellowstone losing its steam? Chloride flux out of Yellowstone National Park. In: Morgan, LA (Ed.), *Integrated Geoscience Studies in the Greater Yellowstone Area: Volcanic, Hydrothermal and Tectonic Processes in the Yellowstone Geocosystem*. U.S. Geol. Surv. Prof. Pap., vol. 1717, pp. 275–297. Chapter I.
- Giggenbach, W.F., 1996. Chemical composition of volcanic gases. In: Scarpa, R., Tilling, R.I. (Eds.), *Monitoring and Mitigation of Volcano Hazards*. Springer Verlag, Berlin, pp. 221–256.
- Giggenbach, W.F., Goguel, R.L., 1989. Collection and analysis of geothermal and volcanic water and gas discharges. Report No. CD2401, New Zealand Department of Scientific and Industrial Research, p. 81.
- Giggenbach, W.F., Sheppard, D.S., Robinson, B.W., Stewart, M.K., Lyon, G.L., 1994. Geochemical structure and position of the Waiotapu geothermal field, New Zealand. *Geothermics* 23, 599–644.
- Goff, F., Janik, C.J., 2002. Gas geochemistry of the Valles caldera region, New Mexico and comparisons with gases at Yellowstone, Long Valley and other geothermal systems. *J. Volcanol. Geotherm. Res.* 116, 299–323.
- Hurwitz, S., Lowenstern, J.B., Heasler, H., 2007a. Spatial and temporal geochemical trends in the hydrothermal system of Yellowstone National Park: inferences from river solute flux. *J. Volcanol. Geotherm. Res.* 162, 149–171. doi:10.1016/j.jvolgeores.2007.01.003.
- Hurwitz, S., Evans, W.C., Lowenstern, J.B., Bergfeld, D., Werner, C., Heasler, H., Jaworowski, C., 2007b. Extensive hydrothermal rock alteration in a low pH, steam-heated environment: Hot Springs Basin, Yellowstone National Park. In: Bullen, T.D., Wang, Y. (Eds.), *Proceedings of the Water–Rock Interaction Symposium-12*, Kunming, China, pp. 81–85.
- Kennedy, B.M., Lynch, M.A., Reynolds, J.H., Smith, S.P., 1985. Intensive sampling of noble gases in fluids at Yellowstone: I. early overview of the data: regional patterns. *Geochim. Cosmochim. Acta* 49, 1251–1261.

- Lehman, J.A., Smith, R.B., Schilly, M.M., Braile, L.W., 1982. Upper crustal structure of the Yellowstone caldera from delay time analyses and gravity correlations. *J. Geophys. Res.* 87, 2713–2730.
- Lewicki, J.L., Bergfeld, D., Cardellini, C., Chiodini, G., Granieri, D., Varley, N., Werner, C., 2005. Comparative soil CO₂ flux measurements and geostatistical estimation methods on Masaya volcano, Nicaragua. *Bull. Volcanol.* doi:10.1007/s00445-005-0423-9.
- Love, J.D., Good, J.M., 1970. Hydrocarbons in Thermal Areas, Northwestern Wyoming. U.S. Geol. Surv. Prof. Pap., vol. 644-B, p. 23.
- Lowenstern, J.B., Janik, C.J., 2003. The origins of reservoir liquids and vapors from The Geysers geothermal field, California (USA). In: Simmons, S.F., Graham, I. (Eds.), *Volcanic, Geothermal and Ore-forming Fluids: Rulers and Witnesses of Processes within the Earth: Soc. of Econ. Geologists Special Pub*, 10, pp. 181–195.
- Lowenstern, J.B., Hurwitz, S., 2008. Monitoring a supervolcano in repose: heat and volatile flux at the Yellowstone Caldera. *Elements* 4 (1), 35–40.
- McCleskey, R.B., Ball, J.W., Nordstrom, D.K., Holloway, J.M., Taylor, H.E., 2005. Water-Chemistry Data for Selected Springs, Geysers, and Streams in Yellowstone National Park Wyoming, 2001–2002. U.S. Geo. Surv. Open-File Report, vol. 2004-1316, p. 94.
- McCrea, J.M., 1950. On the isotopic chemistry of carbonates and a paleotemperature scale. *J. Chem. Phys.* 18, 849–857.
- Miller, D.S., Smith, R.B., 1999. P and S velocity structure of the Yellowstone volcanic field from local earthquake and controlled source tomography. *J. Geophys. Res.* 104, 15,105–15,121.
- Muffler, L.J.P., White, D.E., Truesdell, A.H., 1971. Hydrothermal explosion craters in Yellowstone National Park. *Geol. Soc. Amer. Bull.* 82, 723–740.
- Pierce, K.L., 1974. Surficial geologic map of the Abiathar Peak and parts of adjacent quadrangles, Yellowstone National Park, Wyoming and Montana: Wyoming: U.S. Geol. Surv. Misc. Geol. Invest. Map I-646, Scale 1:62,500.
- Prostka, H.J., Ruppel, E.T., Christiansen, R.L., 1975a. Geologic map of the Abiathar Peak quadrangle, Yellowstone National Park, Wyoming and Montana: U.S. Geol. Surv. Quadrangle Map GQ1244, Scale 1:62,500.
- Prostka, H.J., Smedes, H.W., Christiansen, R.L., 1975b. Geologic map of the Pelican Cone quadrangle, Yellowstone National Park and vicinity, Wyoming. U.S. Geol. Surv. Quadrangle Map GQ1243, Scale 1:62,500.
- Richmond, G.M., 1977. Surficial Geologic Map of the Canyon Village quadrangle, Yellowstone National Park: U.S. Geological Survey Miscellaneous Geologic Investigations Map I-652, Scale 1:62,500.
- Richmond, G.M., Waldrop, H.A., 1972. Surficial geologic map of the Pelican Cone quadrangle, Yellowstone National Park and adjoining area, Wyoming: U.S. Geological Survey Miscellaneous Geologic Investigations Map I-638, Scale 1:62,500.
- Sanders, L.L., 1998. *A Manual of Field Hydrogeology*. Prentice-Hall, Upper Saddle River, NJ, 381 p.
- Smith, R.B., Braile, L.W., 1994. The Yellowstone hotspot. *J. Volcanol. Geotherm. Res.* 61, 121–187.
- Tassi, F., Vaselli, O., Capaccioni, B., Montegrossi, G., Barahona, F., Caprai, A., 2007. Scrubbing process and chemical equilibria controlling the composition of light hydrocarbons in natural gas discharges: an example from the geothermal fields of El Salvador. *Geochem. Geophys. Geosyst.* 8 (5). doi:10.1029/2006GC001487.
- Truesdell, A.H., Fournier, R.O., 1976. Conditions in the Deeper Parts of the Hot Spring Systems of Yellowstone National Park, Wyoming. U.S. Geol. Surv. Open-File report, vol. 76-428, 29 pp.
- Werner, C., Brantley, S., 2003. CO₂ emissions from the Yellowstone volcanic system. *Geochem. Geophys. Geosyst.* 4 (7), 1061. doi:10.1029/2002GC000473.
- Werner, C., Cardellini, C., 2006. Comparison of carbon dioxide emissions with fluid upflow, chemistry, and geologic structures at the Rotorua geothermal system, New Zealand. *Geothermics* 35, 221–238.
- Werner, C., Brantley, S.L., Boomer, K., 2000. CO₂ emissions related to Yellowstone volcanic system 2. Statistical sampling, total degassing, and transport. *J. Geophys. Res.* 105, 10831–10846.
- Werner, C., Christenson, B.W., Hagerty, M., Britten, K., 2006. Variability of volcanic emissions during a crater lake heating cycle at Ruapehu Volcano, New Zealand. *J. Volcanol. Geotherm. Res.* 106, 291–302.
- Werner, C., Hurst, T., Scott, B., Sherburn, S., Christenson, B.W., Britten, K., Cole-Baker, J., Mullan, B., 2008. Variability of passive gas emissions, seismicity, and deformation during crater lake growth at White Island Volcano, New Zealand, 2002–2006. *J. Geophys. Res.* 113, B01204. doi:10.1029/2007JB005094.
- White, D.E., Muffler, L.J.P., Truesdell, A.H., 1971. Vapor-dominated hydrothermal systems compared with hot-water systems. *Econ. Geol.* 66, 75–97.
- White, D.E., Fournier, R.O., Muffler, L.J.P., Truesdell, A.H., 1975. Physical Results of Research Drilling in Thermal Areas of Yellowstone National Park, Wyoming. U.S. Geol. Surv. Prof. Paper, vol. 892, 70 p.
- Xu, Y., Schoonen, M.A.A., Nordstrom, D.K., Cunningham, K.M., Ball, J.W., 1998. Sulfur geochemistry of hydrothermal waters in Yellowstone National Park; I, the origin of thiosulfate in hot spring waters. *Geochim. Cosmochim. Acta* 62, 3729–3743.